Nims, C, et al., 2021, Organic biomorphs may be better preserved than microorganisms in early Earth sediments: Geology, v. 49, https://doi.org/10.1130/G48152.1

## MATERIALS AND METHODS

### Microbial sample collection

Samples of microbial mats dominated by *Thiothrix* sp. – a sulfur-oxidizing, *Gammaproteobacterial* genus (Larkin and Strohl, 1983) – were collected from an abandoned oil and gas well in Centre County, Pennsylvania. Fluorescence *in situ* hybridization (FISH) and cell morphology were used to identify the primary mat populations, as already described in previous work (Nims et al., 2019). An estimated 150 mL of the microbial mat proximal to the sulfidic outflow of the well was pipetted into sterile Falcon tubes in a site visit in February of 2018. The microbial mats were again sampled in April of 2018 to conduct additional silicification experiments. Samples were stored at 5 ˚C with oxygenated headspace in original well water for no more than 7 days. Immediately prior to the silicification procedure, *Thiothrix* samples were centrifuged at low speeds (< 5000 rpm) and rinsed three times with ultrapure 18.2 MΩ water. All samples were manipulated in a biosafety cabinet under laminar flow conditions to minimize contamination.

### Laboratory biomorph synthesis

Organic biomorphs shown in Figure 1 were produced in the laboratory through the slow oxygenation (a few days to a few weeks) of a sterile sulfide solution (500 μM $Na_2S$, Spectrum Chemical) containing yeast extract (1-5 $g.L^{-1}$, Fisher Scientific) or D-glucose (1-5 $g.L^{-1}$, Millipore Sigma) following protocols described in earlier work (Cosmidis and Templeton, 2016; Cosmidis et al., 2019).

For silicification, biomorphs obtained in two weeks in the presence of yeast extract (5 $g.L^{-1}$) were used. The laboratory synthesis of the biomorphs was coordinated with microbial sampling, ensuring synchronized silicification of both fresh biological and abiotic samples. Immediately prior to silicification, biomorphs were collected by centrifugation and rinsed three times with 18.2 MΩ water.

**Silicification protocol**

The experimental parameters were chosen using previously published silicification studies by Toporski et al. (2002) and Benning et al. (2004). Approximately 80 to 100 µL of freshly prepared biomorphs or microbial mat samples were dispensed into sterile, 15 mL Falcon tubes in a biosafety cabinet to avoid sample contamination. We prepared a 10.7 mM sodium meta-silicate solution ($Na_2SiO_3 \cdot 9H_2O$, Fisher Chemical) with 18.2 MΩ water to achieve a concentration of 300 ppm Si (or 642 ppm $SiO_2$) in the silicification medium. The silica concentrations used in this study is an order of magnitude higher than inferred Precambrian open ocean concentrations (> 1.2-2.2 mM Si; Conley et al., 2017)), but could correspond to locally supersaturated ancient chert formation environments (e.g., tidal zones). This concentration of 300 ppm Si was similarly applied in previous experimental silicification studies (Benning et al., 2004). Immediately prior to the onset of silicification experiments, the Si solution pH was adjusted to 7.5 using 2 M HCl, and this solution was filter-sterilized (Whatman® Puradisc 0.2 µm PTFE syringe filters). 8 mL of sterile Si solution were pipetted into individual Falcon tubes containing the dispensed samples under sterile conditions. Each tube was gently agitated to ensure sample coverage and suspension. All samples were stored in a dark cabinet at room temperature (~21˚C). Samples were collected for analyses after an initial 24-hour period, then every week for the first month, followed by every month throughout the rest of the silicification

experiment (up to five months). Weekly pH measurements (InLab Flex-Micro electrode and FiveEasy Plus meter, Mettler Toledo) were recorded over the course of month-long silicification experiments. Both microbial and abiotic silicification experiments had an initial pH of ~7.5.

**Scanning Electron Microscopy**

Scanning electron microscopy (SEM) was used to image both abiotic and microbial samples throughout silicification. Secondary electron images were generated at an accelerating voltage of 5 to 10 kV, with a working distance (WD) of approximately 3 mm, using an FEI Nova NanoSEM630 instrument. Energy dispersive spectroscopy (EDS) analyses were performed at 15 kV and a 5 mm WD using an Oxford Instruments UltimMax detector. The data were analyzed using the Oxford AZtec platform. EDS maps and spectra provided data on the distribution of sulfur and silicon within the samples over the course of the experiments. For SEM/EDS analysis, samples were rinsed with 18.2 MΩ water, and deposited onto 0.22 μm Whatman Nucleopore filters, using a syringe filter holder dispensing system (25 mm, Pall Laboratory). Filters were placed on double-sided carbon tape atop aluminum stubs. All samples were sputter coated with iridium (~12 nm) to prevent charging.

**Transmission Electron Microscopy**

Transmission electron microscopy (TEM) and scanning transmission electron microscopy (STEM) coupled with EDS generated high-resolution images and elemental maps of the samples over the course of silicification. Analyses were conducted using a FEI Talos F200X with an FEG source operating at 200 kV. Images were obtained using a high angle annular dark-field (HAADF) detector in STEM mode. EDS analyses utilized the Super-X EDS system integrated with four silicon drift detectors (SDDs). Chemical maps were constructed using Bruker

QUANTAX ESPRIT software. Samples for TEM analysis were rinsed three times in 18.2 MΩ water and deposited onto a lacey Formvar/Carbon Cu TEM grid (Ted Pella).

**Raman Spectroscopy**

Raman spectroscopy was carried out using a Horiba LabRam HR Evolution Raman Vis-NIR spectrometer coupled with a 633 nm laser source and an Olympus BXFM-ILHS optical microscope and IDS uEye 3 MPix video camera/software. BragGrate notch filters allowed the collection of low frequency (5-10 $cm^{-1}$) signal. The spectra were collected using a groove density of 600 g/mm, and the confocal pinhole aperture was set at 50 μm. A spectral resolution of ~0.8 $cm^{-1}$ was determined by the FWHM of the Rayleigh line. The acquisition range of the spectrometer was centered at 456 $cm^{-1}$ to incorporate anti-Stokes and Stokes measurements (-200 $cm^{-1}$ to 1000 $cm^{-1}$) and verify features in the low frequency range. The spectrometer was calibrated with a silicon standard prior to each Raman session. The point measurements and Raman maps were carried out using either an apochromatic 50x, a long working distance (LWD) 50x, or a 100x objective. This analysis achieved a spatial resolution of approximately 1 μm. Point spectra were collected with two accumulations and 10- to 15-second exposure time. Raman mapping was conducted with one, 10-second accumulation, scanned in defined 0.50-0.80 μm x-y steps on an automated stage. Laser power was approximately 1-1.3 mW at the sample for both single point scans and mapping to avoid sample damage. Several power percentages were tested to optimize laser threshold power.

The LabSpec6 platform was used to process Raman spectra. Spectra were centered according to the position of main peak features in the opposing anti-Stokes and Stokes regions. Baseline correction was performed on raw spectra using polynomial fitting in LabSpec6. Raman mapping incorporated the Classical Least Squares (CLS) fitting function in LabSpec6 to

highlight the distribution of sulfur allotropes within the structures of a mapped region. Overlays of Raman maps on optical images provided visual correlation between the microscopic features and the molecular spectra. Optical microscope images were exported from LabSpec6 and processed using the ImageJ package. Samples were rinsed three times in 18.2 M water prior to Raman spectroscopy. Approximately 20 μL of concentrated sample was pipetted onto glass microscope slides; coverslips prevented samples from drying during analysis.

**Attenuated Total Reflectance Fourier-Transform Infrared Spectroscopy**

Attenuated Total Reflectance Fourier-Transform Infrared spectroscopy (FTIR-ATR) was carried out using a Bruker Vertex V70 spectrometer equipped with a Harrick MVP-Pro Star single-reflection diamond crystal ATR accessory and a liquid nitrogen cooled MCT detector. Spectra were collected from 4000 - 400 $cm^{-1}$, with the integration of 400 sample scans at 6.0 $cm^{-1}$ resolution. Duplicate measurements were made on each sample to ensure spectral consistency. The OPUS 5.5 platform was used to perform baseline correction and evaluate the spectra. Samples for ATR-FTIR were rinsed twice in 18.2 M water and centrifuged into small pellets through the removal of supernatant. Concentrated droplets (10-20 μL) of sample were placed on pre-cut tiles of aluminum foil housed in petri dishes in the biosafety cabinet. Samples dried for 12-24 hours and were analyzed directly on the foil clamped to the ATR diamond.

**X-ray Absorption Near-Edge Structure Spectroscopy at the Sulfur K-edge**

X-ray Absorption Near-Edge Structure Spectroscopy (XANES) spectroscopy at the S K-edge was used to evaluate potential changes in the samples' sulfur redox state and chemical speciation throughout silicification (Jalilehvand, 2006). Samples collected at different times were deposited on 0.2 μm polycarbonate filters (Isopore Membrane Filters, Millipore), rinsed with 18.2 MΩ water, and immediately frozen at -20 °C. The samples were kept frozen until analysis.

XANES spectroscopy was performed on beamline 4-3 of the Stanford Synchrotron Radiation Lightsource (SSRL, Stanford, USA). A liquid He cryostat was used to maintain the temperature at ~25 K during XANES measurements. Analyses were performed in fluorescence-yield mode using a Stern-Heald ionization detector. The Si(111) double crystal monochromator was calibrated using a thiosulfate standard, by setting the position of the maximum of the first pre-edge feature to an energy of 2,472.0 eV. Up to 3 scans per sample were recorded and averaged to improve the signal-to-noise ratio. A linear background determined in the pre-edge region (2400–2470 eV) was subtracted from the averaged data, and the spectra were then normalized at 2510 eV using the Athena program (Ravel and Newville, 2005). Different standards (elemental sulfur, sodium thiosulfate, magnesium sulfate) were run and processed under similar conditions for comparison with the experimental spectra.

**Scanning Transmission X-ray Microscopy**

Scanning Transmission X-ray microscopy (STXM) analyses were performed on beamline 10ID-1 (SM) of the Canadian Light Source (Saskatoon, Canada). The X-ray beam was focused on the samples using a 35 nm Fresnel zone plate objective and an order-sorting aperture for a spot size of ~40 nm on the samples. All samples were analyzed in ~1 atm He. Energy calibration was achieved using the well-resolved 3p Rydberg peak of gaseous $CO_2$ at 294.96 eV. Images, maps and image stacks were acquired in the 390–450 eV (N K-edge), 260–340 eV (C K-edge) and 155–190 eV (S L-edge) energy ranges. The aXis2000 software platform was used for data processing. Maps of elements of interest were obtained by subtracting optical density (OD) images below and at the absorption edge. XANES spectra were extracted from image stacks as described in Cosmidis and Benzerara (2014).

Samples were prepared at different time increments during silicification for STXM analysis. *Thiothrix* and biomorph samples were rinsed three times in 18.2 MΩ water and deposited onto Formvar coated grids (Carbon Type B 200M, Ted Pella) or on $Si_3N_4$ windows (Norcada) to optimize analyses of various elements: S L-edge spectra were measured on Formvar grids, while the C- and N K-edge analyses were conducted on $Si_3N_4$ windows to prevent interference from the Formvar coating. Prior to STXM analyses, grids and windows were evaluated using an optical microscope to pinpoint regions of interest. The nitrogen-carbon (N/C) ratios of the samples were computed using C K- and N K-edge spectra in the 270-453 eV energy range, as described in Alleon et al. (2015).

## SUPPLEMENTARY TEXT

### Sulfur K-edge XANES data interpretation

Particulate materials collected on filters and rinsed with 18.2 MΩ water were analyzed using S K-edge XANES analyses. By comparing the positions of the main absorption peaks in the XANES samples' spectra with that of reference sulfur compounds' spectra, it is possible to qualitatively determine the redox state and speciation of solid sulfur in the samples before and after silicification (Fig. DR3). Prior to silicification, sulfur in both *Thiothrix* and the biomorphs was present mostly as elemental sulfur ($S^0$). After silicification, $S^0$ was still the only form of solid sulfur detected in the *Thiothrix* samples. However, some minor amounts of sulfur corresponding to thiosulfate and sulfate were detected in the spectra of the silicified biomorphs, in addition to $S^0$. The presence of these oxidized forms of inorganic sulfur would indicate sulfur solubilization, oxidation, and reprecipitation during silicification of the biomorphs. However, sulfate and thiosulfate species were not detected in Raman and STXM-based S L-edge XANES analyses, suggesting that these phases represent a minor pool of solid sulfur in these samples. Alternatively, peaks around 2480.8 eV and 2482.5 eV may indicate the presence of organic S-bearing groups such as sulfones and ester sulfates, respectively (Prietzel et al., 2003).

### ATR-FTIR band assignment.

Tentative band assignments for silicifying *Thiothrix* and biomorphs were performed using the results of previous experimental silicification research and IR studies of Si gels (Yoshino et al., 1990; Benning et al., 2004; Orange et al., 2009). Amide absorption bands, which characterize the peptide groups in proteins, are prominent features in *Thiothrix* FTIR spectra. The bending vibrations of amide I (1650 $cm^{-1}$), amide II (1530 $cm^{-1}$), and amide III (1450 $cm^{-1}$) bands shift approximately 10 wavenumbers higher in the silicified *Thiothrix* samples. A broad, intensifying

siloxane band overlaps the other polysaccharide peaks diagnostic of the *Thiothrix* membrane and sheath structures at 1050 $cm^{-1}$, which can be attributed to asymmetric Si-O stretching (Fig. DR4A). A distinct band related to silica polymerization develops at 800 $cm^{-1}$, likely the intra-tetrahedral stretch of Si-O-Si bonds, increases in intensity and signifies the probable formation of amorphous Si gel sorbing to the cell sheath.

Some 400 to 500 $cm^{-1}$ bands appear in the *Thiothrix* samples. A band at 473 $cm^{-1}$ is tentatively assigned to the S-S bond stretching of S(0) (Meyer, 1976). This band is present in the non-silicified and one-week silicified *Thiothrix* sample, but it shifts into higher wavenumbers after a month of silicification. Silica gel vibrations, including Si-O-Si stretching modes at 576 $cm^{-1}$, could also contribute to the small peak in this region (Nariyal et al., 2014)

Abiotic biomorphs also display significant spectral changes during silicification (Fig. DR4B). Biomorphs FTIR spectra include a 950 $cm^{-1}$ feature, which could indicate the C-O stretch of alcohols and aliphatic ethers, and band around 1550-1675 $cm^{-1}$, which could be assigned to C=O stretching and C=C stretching, as described in earlier studies (Cosmidis et al., 2019). A small feature at 1248 $cm^{-1}$ could represent carboxylic acids

Silicification amplifies the intensity of existing bands in the organic biomorph samples and introduces new silica-related features (Fig. DR4B). During silicification, the O-H stretch (3280 $cm^{-1}$) increases in intensity, along with the appearance of a 1645 $cm^{-1}$ band. This feature could indicate the presence of more hydrated species, silanols (Si-OH), in the silicifying biomorphs (Benning et al., 2004). The inter-tetrahedral stretch of the Si-O band appears at 1105 $cm^{-1}$ and is positioned relatively higher in the biomorphs based on the coincident polysaccharide peak in the microbial samples. A broadening and intensifying of the absorption band at 1385 $cm^{-1}$ throughout silicification could represent the S=O stretch of sulfates and sulfonic groups. The

feature at 800 $cm^{-1}$ associated with Si-O-Si bonds is absent in biomorphs samples, appearing only as a shoulder in the monthlong silicified measurement.

Low frequency bands (500 $cm^{-1}$ to 700 $cm^{-1}$) in the silicified biomorphs could be interpreted as the skeletal vibration of the 4-fold siloxane ring (Yoshino et al., 1990). Centered around 560 $cm^{-1}$, this band could alternately be ascribed to sulfur and the stretching vibrations of C-S functional groups (Bastian and Martin, 1973; McNamara et al., 2016). The development of this C-S stretching band may indicate the extensive sulfurization of the biomorph organics during silicification.

Silicified *Thiothrix* and biomorphs present prominent reststrahlen bands at 450 $cm^{-1}$, marked by a dashed red box in Fig. DR4. The ATR spectral cut-off range in the same region hinders clear interpretation of this band, but it could be associated with the sulfur content in both samples. Mineral inclusions can become strong reflectors near an absorption band, and thus can present the reststrahlen effect. It is possible that the presence of sulfur in the samples could cause this spectral band reversal (Gulley-Stahl et al., 2010).

**STXM C K-edge & N K-edge data interpretation**

At the C K-edge, non-silicified *Thiothrix* samples present characteristic peaks of microbial cells (Benzerara et al., 2004; Chan et al., 2011): small peaks at 285.1 eV and 285.5 eV ($1s \rightarrow \pi^*_{C=C}$ transitions of unsaturated or aromatic C), a shoulder feature around 287.1-287.3 eV ($1s \rightarrow \pi^*$ transitions in phenols and ketones and $1s \rightarrow \sigma$ transitions in aliphatics), a pronounced peak at 288.2 eV ($1s \rightarrow \pi^*_{C=O}$ transitions in amide groups), a shoulder at 288.5 eV ($1s \rightarrow \pi^*_{C=O}$ transitions in carboxylic groups) and a small peak around 289.3-289.6 eV ($1s \rightarrow 3p/\sigma^*$ transitions of alcohols, ethers, hydroxylated aliphatics).

Prior to silicification, a feature at 288.5 eV (carboxylic groups) is predominant in the spectra of the biomorphs. Smaller absorption features at 285.1 eV and 285.5 eV (unsaturated carbon and aromatics), 289.3-289.6 eV (alcohols and ethers), and shoulders at 287.1-287.3 eV (phenols/ ketones and aliphatics) are also present in the spectra of the non-silicified biomorphs.

C K-edge spectra of one-week silicified *Thiothrix* and biomorphs samples reveal early alteration to the organic constituents in both samples. The main change in the spectra of the silicifying *Thiothrix* is the relative intensification of the peak at 288.5 eV (carboxylic groups), while the small peak around 289.3-289.6 eV (alcohols and ethers) becomes weaker. In contrast, the characteristic peak of carboxylic groups (288.5 eV) broadens and diminishes in intensity in the silicifying biomorphs sample. Moreover, the shoulder at 285.5 eV indicative of unsaturated or aromatic carbon in the biomorphs becomes more prominent during silicification of the biomorphs. Finally, a shoulder feature around 287.7 eV (1s→3p/σ* transitions in aliphatics), as well as a small absorption feature at 290.6 eV (1s→4p/σ* transitions in aliphatics) indicate a higher proportion of aliphatics in the silicified biomorphs relative to the non-silicified biomorphs.

At the N K-edge, a sharp peak at ~401.2 eV in the non-silicified and silicified Thiothrix spectra could be attributed to amide groups (Leinweber et al., 2007), which is typical of bacterial samples (Alleon et al., 2017). The N K-edge spectra of the biomorph samples present broad absorption steps lacking diagnostic features of nitrogen-bearing species, making difficult to evaluate the contributions from organic and inorganic forms.

**SUPPLEMENTARY FIGURES**

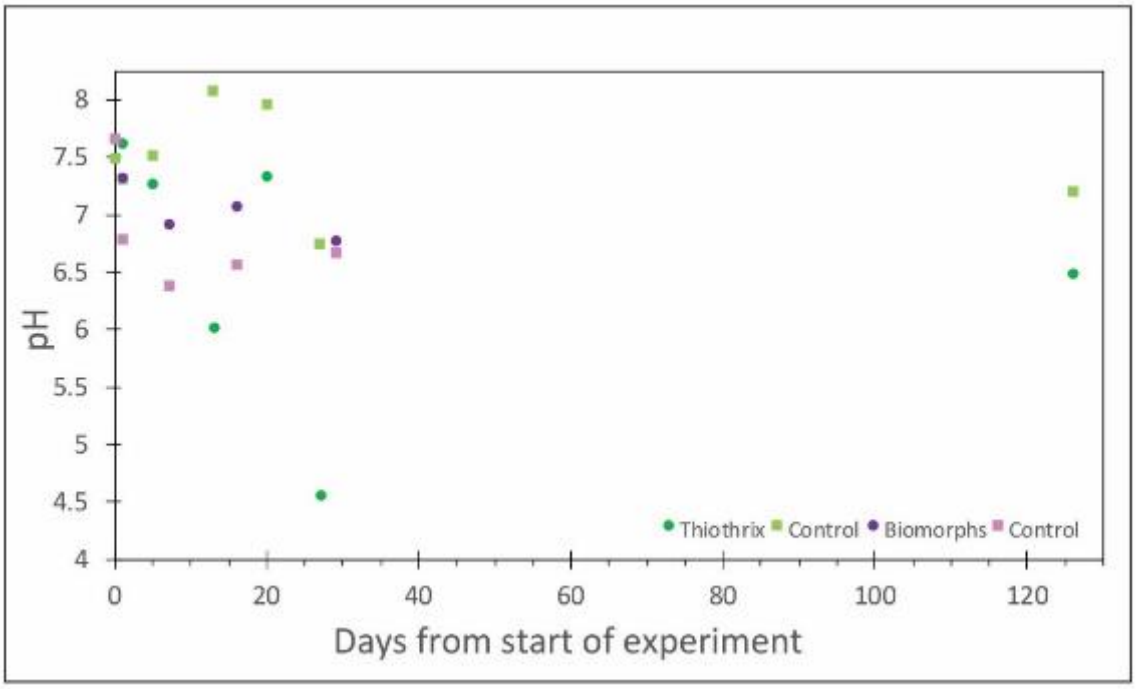


Figure DR1. pH measurements of the experimental silicification media. Measurements were recorded at 24-hours, followed by weekly measurements. Green and purple circle markers indicate the *Thiothrix* or biomorph samples respectively, while square markers indicate controls without *Thiothrix* or biomorphs (i.e., the sodium metasilicate medium used in silicification experiment).

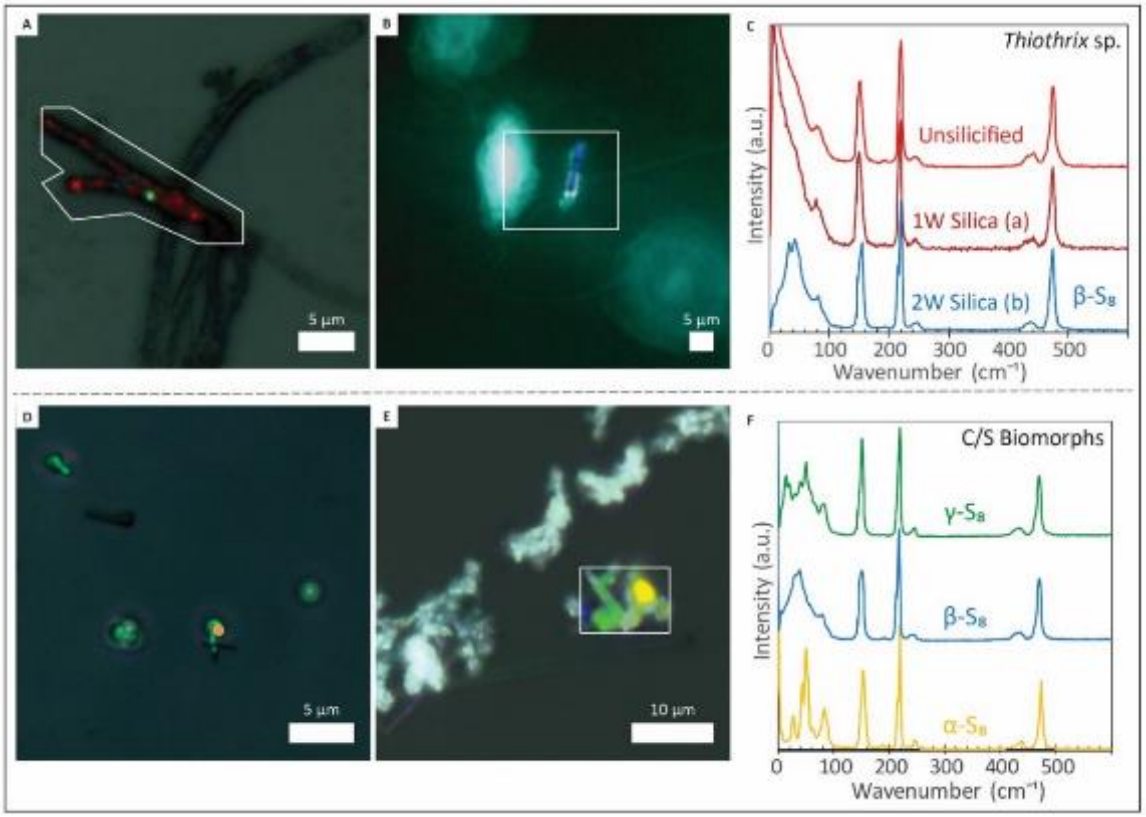


Figure DR2. Raman map overlays on optical microscope images, of (A) one-week silicifying *Thiothrix* (white polygon); (B) two-week silicifying *Thiothrix* (white rectangle); (C) *Thiothrix* Raman spectra; (D) location of point spectrum (orange marker) of non-silicified biomorphs characterized by γ-$S_8$; (E) Raman map overlay (white rectangle) on optical microscope image of two-month silicifying biomorphs; (F) corresponding biomorph Raman spectra. Mapped colors correspond to color of plotted spectrum. Amorphous intracellular biosulfur is mapped in red and crystalline sulfur allotropes, β-$S_8$, γ-$S_8$, α-$S_8$, are mapped in blue, green, and yellow respectively.

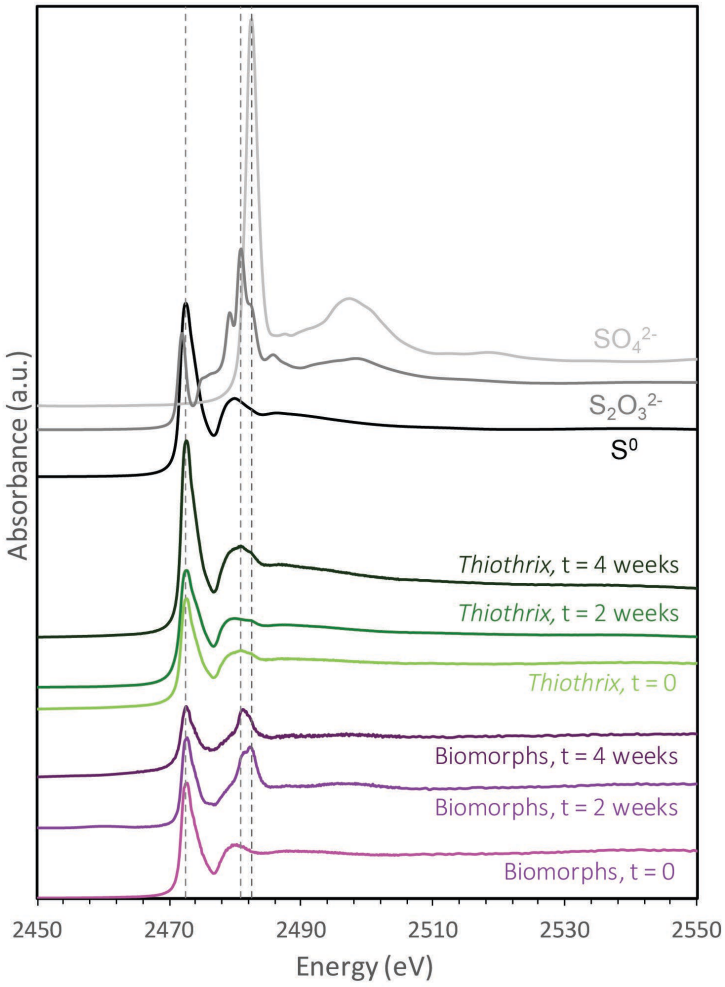


Figure DR3. S K-edge XANES analyses of non-silicified and silicified biomorphs and *Thiothrix.* Samples were analyzed before silicification (t = 0) and after 2 and 4 weeks of silicification. The spectra are plotted along with reference spectra for elemental sulfur ($S^0$), thiosulfate ($S_2O_3^{2-}$) and sulfate ($SO_4^{2-}$). Dashed vertical line correspond to 2472.4 (maximum absorption for S0), 2480.8 (maximum absorption for $S_2O_3^{2-}$), and 2482.5 eV (maximum absorption for $SO_4^{2-}$).

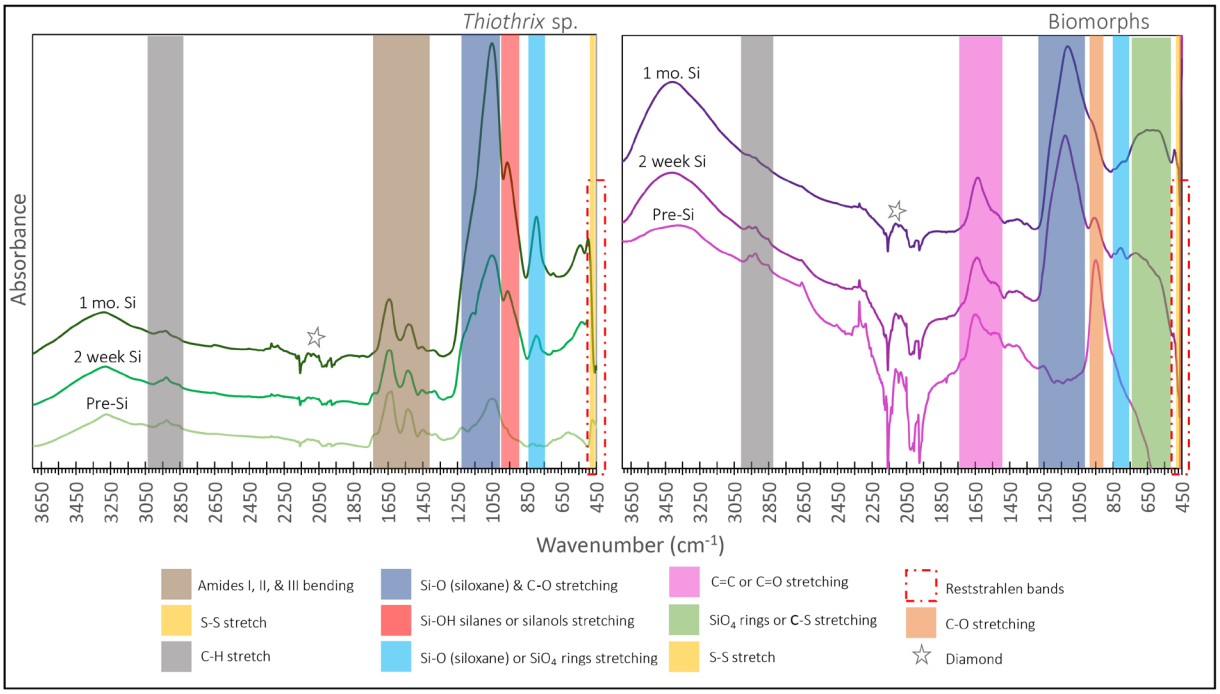


Figure DR4. FTIR-ATR absorbance spectra of non-silicified, two-week silicified, and one-month silicified samples: (A) *Thiothrix* spectra; (B) Organic biomorphs spectra. Spectra were normalized to the 1650 $cm^{-1}$ feature. Color key defines tentative band assignments. See supplementary text for interpretation.

**REFERENCES CITED**


Alleon, J., Bernard, S., Le Guillou, C., Daval, D., Skouri-Panet, F., Kuga, M., and Robert, F., 2017, Organic molecular heterogeneities can withstand diagenesis: Scientific Reports, v. 7, p. 1–9, doi:10.1038/s41598-017-01612-8.

Alleon, J., Bernard, S., Remusat, L., and Robert, F., 2015, Estimation of nitrogen-to-carbon ratios of organics and carbon materials at the submicrometer scale: Carbon, v. 84, p. 290–298, doi:10.1016/j.carbon.2014.11.044.

Bastian, E.J., and Martin, R.B., 1973, Disulfide vibrational spectra in the sulfur-sulfur and carbon-sulfur stretching region: The Journal of Physical Chemistry, v. 77, p. 1129–1133, doi:10.1021/j100628a010.

Benning, L.G., Phoenix, V.R., Yee, N., and Konhauser, K.O., 2004, The dynamics of cyanobacterial silicification: An infrared micro-spectroscopic investigation: Geochimica et Cosmochimica Acta, v. 68, p. 743–757, doi:10.1016/S0016-7037(03)00488-5.

Benzerara, K., Yoon, T.H., Tyliszczak, T., Constantz, B., Spormann, A.M., and Brown, G.E., 2004, Scanning transmission X-ray microscopy study of microbial calcification: Geobiology, v. 2, p. 249–259, doi:10.1111/j.1472-4677.2004.00039.x.

Chan, C.S., Fakra, S.C., Emerson, D., Fleming, E.J., and Edwards, K.J., 2011, Lithotrophic iron-oxidizing bacteria produce organic stalks to control mineral growth: implications for biosignature formation: The ISME Journal, v. 5, p. 717–727, doi:10.1038/ismej.2010.173.

Conley, D.J., Frings, P.J., Fontorbe, G., Clymans, W., Stadmark, J., Hendry, K.R., Marron, A.O., and De La Rocha, C.L., 2017, Biosilicification Drives a Decline of Dissolved Si in the Oceans through Geologic Time: Frontiers in Marine Science, v. 4, p. 397, doi:10.3389/fmars.2017.00397.

Cosmidis, J., and Benzerara, K., 2014, Soft X-ray Scanning Transmission Spectromicroscopy, *in* Biomineralization Sourcebook: Characterization of Biominerals and Biomimetic Materials, London, UK, E. DiMasi and L.B. Gower, p. 115–133.

Cosmidis, J., Nims, C.W., Diercks, D., and Templeton, A.S., 2019, Formation and stabilization of elemental sulfur through organomineralization: Geochimica et Cosmochimica Acta, v. 247, doi:10.1016/j.gca.2018.12.025.

Cosmidis, J., and Templeton, A.S., 2016, Self-Assembly of biomorphic carbon/sulfur microstructures in sulfidic environments: Nature Communications, v. 7, p. 1–9, doi:10.1038/ncomms12812.

Gulley-Stahl, H.J., Bledsoe, S.B., Evan, A.P., and Sommer, A.J., 2010, The Advantages of an Attenuated Total Internal Reflection Infrared Microspectroscopic Imaging Approach for

Kidney Biopsy Analysis: Applied Spectroscopy, v. 64, p. 15–22, doi:10.1366/000370210792966161.

Jalilehvand, F., 2006, Sulfur: not a “silent” element any more: Chemical Society Reviews, v. 35, p. 1256, doi:10.1039/b417595f.

Larkin, J.M., and Strohl, W.R., 1983, Beggiatoa, Thiothrix, and Thioploca: Annual Review of Microbiology, v. 37, p. 341–367, doi:10.1146/annurev.mi.37.100183.002013.

Leinweber, P., Kruse, J., Walley, F.L., Gillespie, A., Eckhardt, K.U., Blyth, R.I.R., and Regier, T., 2007, Nitrogen K-edge XANES - An overview of reference compounds used to identify “unknown” organic nitrogen in environmental samples: Journal of Synchrotron Radiation, v. 14, p. 500–511, doi:10.1107/S0909049507042513.

McNamara, M.E., van Dongen, B.E., Lockyer, N.P., Bull, I.D., and Orr, P.J., 2016, Fossilization of melanosomes via sulfurization (A. Smith, Ed.): Palaeontology, v. 59, p. 337–350, doi:10.1111/pala.12238.

Meyer, B., 1976, Elemental sulfur: Chemical Reviews, v. 76, p. 367–388, doi:10.1021/cr60301a003.

Nariyal, R.K., Kothari, P., and Bisht, B., 2014, FTIR Measurements of SiO2 Glass Prepared by Sol-Gel Technique: Chemical Science Transactions, v. 3, p. 1064–1066, doi:10.7598/cst2014.816.

Nims, C., Cron, B., Wetherington, M., Macalady, J., and Cosmidis, J., 2019, Low frequency Raman Spectroscopy for micron-scale and in vivo characterization of elemental sulfur in microbial samples: Scientific Reports, v. 9, p. 7971, doi:10.1038/s41598-019-44353-6.

Orange, F., Westall, F., Disnar, J.-R., Prieur, D., Bienvenu, N., Le Romancer, M., and Défarge, C., 2009, Experimental silicification of the extremophilic Archaea Pyrococcus abyssi and Methanocaldococcus jannaschii: applications in the search for evidence of life in early Earth and extraterrestrial rocks: Geobiology, v. 7, p. 403–418, doi:10.1111/j.1472-4669.2009.00212.x.

Prietzel, J., Thieme, J., Neuhäusler, U., Susini, J., and Kögel-Knabner, I., 2003, Speciation of sulphur in soils and soil particles by X-ray spectromicroscopy: European Journal of Soil Science, v. 54, p. 423–433, doi:https://doi.org/10.1046/j.1365-2389.2003.00543.x.

Ravel, B., and Newville, M., 2005, ATHENA, ARTEMIS, HEPHAESTUS: data analysis for X-ray absorption spectroscopy using IFEFFIT: Journal of Synchrotron Radiation, v. 12, p. 537–541, doi:10.1107/S0909049505012719.

Toporski, J.K.W., Steele, A., Westall, F., Thomas-Keprta, K.L., and McKay, D.S., 2002, The simulated silicification of bacteria--new clues to the modes and timing of bacterial preservation and implications for the search for extraterrestrial microfossils: Astrobiology, v. 2, p. 1–26.

Yoshino, H., Kamiya, K., and Nasu, H., 1990, IR study on the structural evolution of sol-gel derived SiO2 gels in the early stage of conversion to glasses: Journal of Non-Crystalline Solids, v. 126, p. 68–78, doi:10.1016/0022-3093(90)91024-L.